Hyperfine interactions at ^{181}Hf($\rightarrow^{181}$Ta) impurities implanted in Er$_2$O$_3$ and Gd$_2$O$_3$: structural and electronic dependence of the EFG in bixbyite sesquioxides

L.A. Errico[1], M. Rentería[1,2,a], A.F. Pasquevich[1], A.G. Bibiloni[1], and K. Freitag[3]

[1] Departamento de Física e Instituto de Física La Plata (IFLP, CONICET), Facultad de Ciencias Exactas,
Universidad Nacional de La Plata, CC 67, 1900 La Plata, Argentina
[2] Laboratoire pour l'Utilisation du Rayonnement Électromagnétique (LURE), Centre Universitaire Paris-Sud,
bâtiment 209 A, BP 34, 91898, Orsay Cedex, France
[3] Institut für Strahlen-und Kernphysik (ISKP) der Universität Bonn, Nussallée 14-16, 53115 Bonn, Germany

Abstract. The time-differential-perturbed γ-γ angular-correlation technique (TDPAC) with ion-implanted ^{181}Hf tracers has been applied to study the hyperfine interactions of ^{181}Ta impurities in the cubic bixbyite structure of Er$_2$O$_3$ and Gd$_2$O$_3$. The TDPAC experiments were performed in air in the temperature range 300–1073 K (in the case of Er$_2$O$_3$) and 300–1173 K (in the case of Gd$_2$O$_3$). Three electrical-quadrupole interactions were found in each oxide in the whole studied temperature range. Two of them were attributed to the electric-field gradients (EFG) acting on ^{181}Ta probes substitutionally located on the two nonequivalent free-of-defects cation sites of the bixbyite structure. The EFG results are compared with predictions of the point-charge model and discussed together with previous results obtained with the probes ^{111}Cd and ^{181}Ta in other isomorphous sesquioxides. The temperature dependence of the hyperfine parameters for both oxides is also discussed in terms of dilatometric expansion data.

1 Introduction

In the last years, the time-differential γ-γ perturbed-angular-correlation (TDPAC) technique has been increasingly applied in the solid-semiconductor research being nowadays widely recognised as a powerful tool for the study of different properties of semiconductors and insulators [1]. To take advantage of the possibilities of the technique, the parameters that characterise hyperfine interactions of adequate probes suitably located in the system under study should be determined.

The technique is based on the observation of the influence of extranuclear fields on the correlation between the emission directions of two successive gamma-radiations emitted during a nuclear-decay cascade. The method requires, in the case of metal oxides, the introduction of an adequate radioactive probe (generally an impurity) in substitutional cation sites of the lattice. When the interest is focused in the electric-field gradient (EFG) tensor it can be determined, if the nuclear-quadrupole moment of the intermediate level of the cascade is known, through

[a] e-mail: `renteria@venus.fisica.unlp.edu.ar`

the measurement of the nuclear-quadrupole frequency ω_Q and the asymmetry parameter η.

A large number of experimental EFG's measured with the TDPAC technique at the site of the ^{111}Cd impurity in binary oxides has been the object of different analysis in order to obtain semiempirical models that can describe the different contributions to the EFG at the impurity sites [2–7].

To study the influence of the electronic configuration of the impurity probe-atom itself on the EFG it is essential to perform TDPAC measurements with different probes in isomorphous crystal structures. In TDPAC experiments the most commonly used radioactive probe, apart from the already mentioned ^{111}Cd, is ^{181}Ta, which has quite a different electronic configuration from that of cadmium. Hence, the extension of the systematic analysis made with ^{111}Cd to this second probe looks of great interest [8–11]. With this purpose, in 1994, we started a systematic study of one of the binary oxides group, *i.e.*, the bixbyites, using ^{181}Ta as probe [12]. This group was the subject of several investigations using ^{111}Cd as probe [13] and presents a particular interest since its crystalline structure has two nonequivalent sites for cations with quite different coordination symmetry.

In this context, we performed TDPAC experiments in two sesquioxides that crystallise in the bixbyite structure, namely in ^{181}Hf($\rightarrow^{181}$Ta)-implanted Er_2O_3 and Gd_2O_3 in the temperature range 300–1073 K (Er_2O_3) and 300–1173 K (Gd_2O_3), focusing attention to probe-atoms substitutionally located at both nonequivalent free-of-defects cationic sites of the structure. These results, along with those obtained for the rest of the ^{181}Ta-bixbyite systematics, enable us to discuss the possible dependences of the EFG on the electronic configuration of the probes and on their coordination geometry with the oxygen nearest-neighbour (NN) atoms through the comparison with point-charge model (PCM) predictions and with the ^{111}Cd systematics in bixbyites.

The experimental procedure as well as a brief description of the TDPAC technique and the general characteristics of the bixbyite structure related with the contribution to the EFG are described in Section 2. In Section 3 we present the experimental results and in Section 4 we discuss the assignment of the interactions, its temperature dependence, and some trends that come out from their comparison to previous data and theoretical predictions. Finally, in Section 5 we summarise and present our conclusions.

2 Experimental

2.1 Basic principles of the TDPAC technique, experimental setup and data reduction

As the TDPAC technique and its applications has been reviewed extensively in the literature (see for example Refs. [14–16]), only a brief description of the method and the experimental setup used in these experiments will be given here. The TDPAC spectroscopy reflects the local electronic environment of an adequate probe nucleus, introduced in the system under study, *via* the hyperfine interaction with external electric-field gradients. The EFG results from the charge density distribution that in turn depends on the electronic characteristics of the atomic surroundings and on the nature of chemical bonds. The EFG is usually characterised by the nuclear-quadrupole frequency $\omega_Q = eQV_{ZZ}/40\hbar$ and the asymmetry parameter $\eta = (V_{YY} - V_{XX})/V_{ZZ}$, where V_{ii} are the principal components of the EFG tensor arbitrarily named in order that $|V_{XX}| < |V_{YY}| < |V_{ZZ}|$. The quadrupole frequency ω_Q gives information about the strength of the EFG, while an asymmetry parameter $\eta > 0$ reflects a deviation from axial symmetry ($\eta = 0$).

The hyperfine electric-nuclear-quadrupole interaction is traced *via* a γ-γ cascade of a radioactive decay. The time-modulated probability to detect, at a time t, the second γ-ray at an angle θ with respect to the direction of emission of the first γ-ray is given by [14]:

$$W(\theta, t) = 1 + A_{22} G_{22}(t) P_2(\cos\theta), \qquad (1)$$

where A_{22} is the anisotropy of the γ-γ cascade that depends on the nuclear properties only and $P_2(\cos\theta)$

is the second-order Legendre polynomial. In the case of pure electric-quadrupole interaction the perturbation function $G_{22}(t)$ contains all the information of the hyperfine interactions between the nuclear-electric-quadrupole moment eQ and an extra-nuclear EFG.

For polycrystalline samples and a nuclear spin $I = 5/2$ of the intermediate nuclear level of the cascade, the perturbation factor $G_{22}(t)$ for static electric-quadrupole interactions has the form [14]:

$$G_{22}(t) = \sum_i f^i \left(S_{20,i} + \sum_{n=1}^{3} \left[S_{2n,i} \cos(\omega_{ni}t) \, e^{-\delta_i \omega_{ni} t} \right] \right), \qquad (2)$$

where f^i is the relative fraction of nuclei that experiments a given perturbation. The ω_n frequencies are related to the quadrupole frequency ω_Q by $\omega_n = g_n(\eta)\omega_Q$. The g_n and S_{2n} coefficients are known functions [17] of the asymmetry parameter η. The exponential functions account for a Lorentzian frequency distribution of relative width δ around ω_n.

In this work we made use of the well-known 133–482 keV γ-γ cascade in ^{181}Ta produced after the β^- nuclear decay of ^{181}Hf. A conventional fast-fast coincidence system with four BaF_2 detectors in a coplanar 90° arrangement, with a time resolution of 0.9 ns, was used for data acquisition. Eight coincidence spectra, $C_{ij}(t)$, four taken between detectors positioned with 180° symmetry and four of eight possible with 90° symmetry, were simultaneously recorded in an 8 K-memory multichannel analyser. These coincidence spectra (corrected for accidental events) were used to generate the experimental asymmetry ratio $R(t)$ [18]:

$$R(t) = 2 \frac{(C_{13}(t)C_{24}(t))^{1/2} - (C_{14}(t)C_{23}(t))^{1/2}}{(C_{13}(t)C_{24}(t))^{1/2} + 2(C_{14}(t)C_{23}(t))^{1/2}}$$
$$\approx A_{22}^{\text{exp}} G_{22}(t), \qquad (3)$$

where A_{22}^{exp} is the effective anisotropy of the cascade for a given experimental condition. To extract the experimental hyperfine parameters ω_Q and η theoretical functions of the form $A_{22}^{\text{exp}} G_{22}(t)$ (using the expressions of Eq. (2)), folded with the time-resolution curve, were fitted to the experimental $R(t)$ asymmetry ratio.

2.2 The Bixbyite structure. Consequences on the EFG's and point charge model predictions

Fe, Mn, Sc, In, Tl, Y, and all the rare-earth elements, under suitable conditions, form a sesquioxide M_2O_3. Polymorphism is common and below about 2300 K, three polymorphous crystallographic structures have been found: the hexagonal-A, monoclinic-B, and cubic-C form (bixbyite) [19].

The cubic form takes its name from the mineral (Fe, Mn)$_2O_3$, called bixbyite. In this structure, the cations form a nearly cubic face-center lattice (space group Ia3) in which six out of the eight tetrahedral sites are occupied

by oxygen atoms. The unit cell of the oxide crystal structure consists of eight such cubes, containing 32 cations and 48 O^{-2} ions. Two nonequivalent cation sites, called "C" and "D", both with 6-fold oxygen coordination, characterise the structure. Their relative abundance in the lattice is $f^C/f^D = 3$. Site D is axially symmetric and can be described as a cation surrounded by six oxygen atoms at the corners of a distorted cube, leaving two corners of the same diagonal free. In site C the cube is more distorted and the six oxygen atoms leave free two corners on a face diagonal. Therefore we expect two clearly distinguishable hyperfine interactions. That corresponding to site C will be characterised by $\eta^C \neq 0$, while $\eta^D \approx 0$ will characterised the axially symmetric one corresponding to site D. According to their relative abundances, the first one should be present with more intensity.

It is well known that the bonding in these sesquioxides is mainly ionic [20]. Under such conditions, the PCM [2,12] should be a good starting model to evaluate the EFG parameters at the two sites C and D. Using the lattice parameters and the atomic coordinates coming from the most accurate X-ray determinations quoted in the literature [21] and $\gamma_\infty = -61.42$ [22], the results of the PCM calculation (using a sphere radius of 20 nm) for both sites in Er$_2$O$_3$ are: $\omega_Q^C = -10.84$ Mrad/s, $\eta^C = 0.72$ and $\omega_Q^D = +24.61$ Mrad/s, $\eta^D = 0.0$. The results for Gd$_2$O$_3$ are: $\omega_Q^C = -10.32$ Mrad/s, $\eta^C = 0.62$ and $\omega_Q^D = +26.81$ Mrad/s, $\eta^D = 0.0$. According to these results and the geometry of the two nonequivalent cationic sites we should expect experimental values close to 0 for η^D and $\eta^C > 0.6$. In addition we should expect $\omega_Q^D \cong 2\omega_Q^C$.

2.3 Sample preparation and measurements

Commercially-obtained high-purity Er$_2$O$_3$ and Gd$_2$O$_3$ powder samples (Aldrich, 99.99% and 99.9% metallic purity, respectively) were pressed in circular pellets and sintered in air for 2.5 h at 1273 K. In both cases, X-ray diffraction analysis of the samples verified that only the crystalline C-phase was present after the mentioned treatments. The ion accelerator of the Institut für Strahlen- und Kernphysik (ISKP, Bonn) was then used to implant ^{181}Hf$^+$ ions into the samples with the following energies and doses: Er$_2$O$_3$, 150 keV and 5×10^{13} ions/cm^2; Gd$_2$O$_3$, 150 keV and 1.3×10^{14} ions/cm^2.

The TDPAC measurements were performed first at room temperature (RT = 300 K) in air in the as-implanted samples, in order to establish the initial degree of substitution of the impurities, the magnitude of the radiation damage and the hyperfine interactions present before any thermal treatment of the samples. After these measurements, both samples underwent annealing treatments in air at 1173 K during 2 h and 24 h for Er$_2$O$_3$ and Gd$_2$O$_3$, respectively. Afterwards, TDPAC measurements were carried out in air between 300 and 1073 K with 100 K steps in the case of Er$_2$O$_3$, and at 300, 423, 573, 723, 873, 1023 and 1173 K in the case of the Gd$_2$O$_3$ sample. The typical elapsed time for these measurements was 24 h.
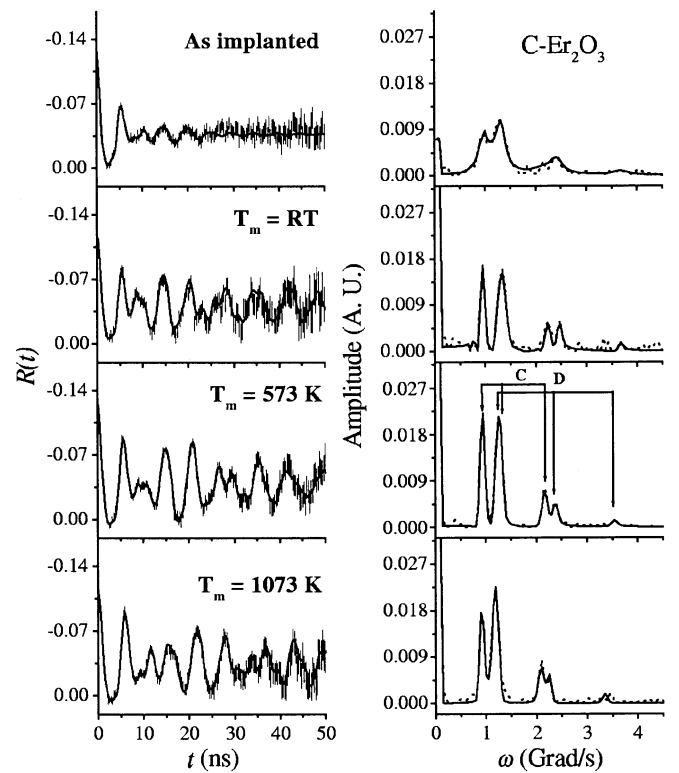

Fig. 1. $R(t)$ spectra (left) and their corresponding Fourier transforms (right) of $(^{181}\text{Hf} \rightarrow)^{181}\text{Ta}$ in cubic Er$_2$O$_3$ measured at RT as implanted and after thermal annealing in air at 1173 K × 2 h, at the indicated measuring temperature T_m. Solid lines in the $R(t)$ spectra are least-squares fits of equation (3) to the experimental data. Solid lines in the Fourier spectra come from the Fourier transform of the $R(t)$ fits. The frequencies ω_n associated with the hyperfine interactions Hfi C and Hfi D are indicated in the third Fourier transform.

Powder X-ray diffraction (XRD) measurements were done in the ^{181}Hf-implanted Gd$_2$O$_3$ sample after its radioactive decay, and in an identical sample mixed with 10% of monoclinic B-Gd$_2$O$_3$ high-temperature phase.

3 Results

Figures 1 and 2 show the $R(t)$ spectra, and their corresponding Fourier transforms, taken on both as-implanted samples at RT in air and the more relevant spectra taken after annealing of the samples. The parameter values of the two fitted hyperfine interactions in the as-implanted spectra, labelled Hfi C and Hfi D, are listed in Table 1 for both oxides as well as the parameters of the two main and well-defined interactions found in the after-annealing spectra taken at RT. A close inspection of the $R(t)$ spectra reveals that the experimental anisotropy A_{22}^{exp} (between 0.11–0.16) is lower than the value of 0.20 expected for the geometry and time-resolution of the measurement. However, the "hard-core" value $R(t = \infty) \cong 0.04$ observed in the as-implanted samples corresponds to such expected anisotropy. This indicates that the lost of amplitude at $t = 0$ must be originated in a fraction of probes that feels

Table 1. Results of least-squares fits of equation (3) to the $R(t)$ spectra, displayed in Figures 1 and 2, taken at room temperature. When no errors are quoted it means that the parameter was kept fixed. The fractions $f^C + f^D$ are normalized to 100% in the after-annealing results and in the as-implanted result in the case of Gd_2O_3 (see text).

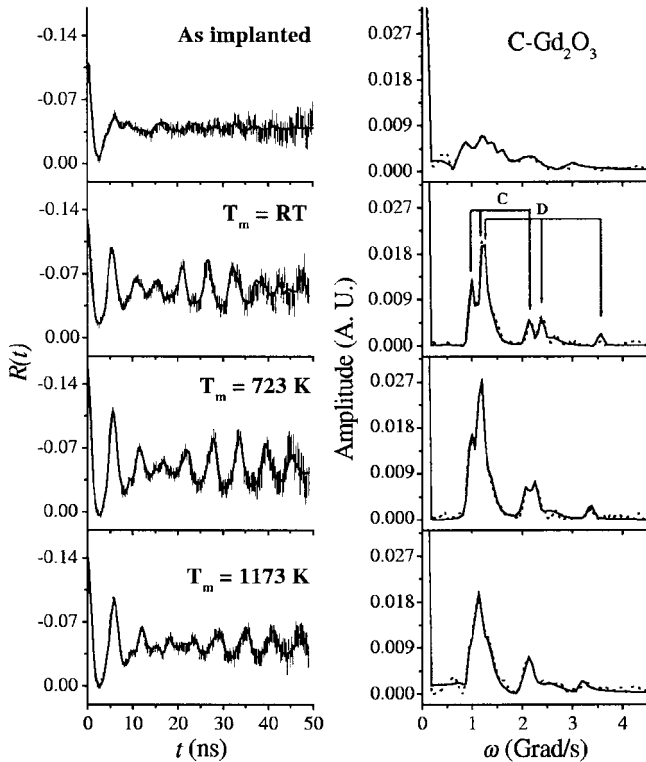| Oxide	Hfi C				Hfi D			
	f	ω_Q (Mrad/s)	η	$\delta(\%)$	f	ω_Q (Mrad/s)	η	$\delta(\%)$
Er_2O_3								
As implanted	72_3	111_1	0.68_2	13_1	28_1	202_2	0.23_2	4.9_8
After annealing	69_2	115.6_5	0.570_6	1.4_4	31_2	203.7_8	0	0.8_6
Gd_2O_3								
As implanted	66_3	94.3_9	0.64_1	13_1	34_3	176_2	0.32_2	8.1_9
After annealing	74_3	105.8_3	0.768_4	1.6_3	26_1	197.9_5	0	1.6_3

Fig. 2. $R(t)$ spectra (left) and their corresponding Fourier transforms (right) of $(^{181}\text{Hf} \rightarrow)^{181}\text{Ta}$ in cubic Gd_2O_3 measured at RT as implanted and after thermal annealing in air at 1173 K $\times$ 24 h, at the indicated measuring temperature T_m. Solid lines in the $R(t)$ spectra are least-squares fits of equation (3) to the experimental data. Solid lines in the Fourier spectra come from the Fourier transform of the $R(t)$ fits. The frequencies ω_n associated with the hyperfine interactions Hfi C and Hfi D are indicated in the second Fourier transform.

a very high ω_Q frequency not resolved within the time resolution of the spectrometer. In the text all the fractions are related to the number of probes that sense a resolved hyperfine interaction, *i.e.* between 55% and 80% of the total number of implanted impurities.
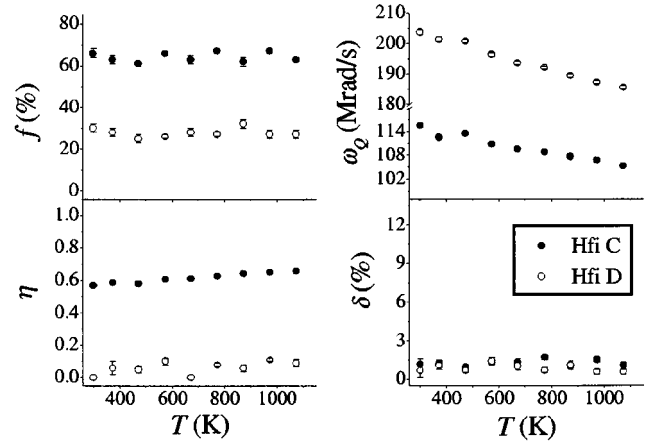

Fig. 3. Evolution of the hyperfine parameters of interactions Hfi C and Hfi D found in C-Er_2O_3 as a function of the measuring temperature T.

As can be seen from Figures 1 and 2 the $R(t)$ as-implanted spectra are rather dampened, as usually occurs in the as-implanted stage of impurity-implanted binary oxides [12,18,23], showing that the radiation damage produces a not negligible host disorder around the probe-atoms. But, at the same time, the values of the hyperfine signals and the almost random distribution of the probes (as-implanted fractions are nearly in a 3:1 ratio) show a high degree of impurity substitution at cationic sites. In effect, already in this stage it is possible to detect almost the same ω_n frequencies corresponding to Hfi C and Hfi D that will be found after the annealing treatments (see Figs. 1 and 2, first and second Fourier spectra), but with a rather broad frequency distribution.

After the annealing treatment, these two interactions are well defined ($\delta < 2\%$) and amount to almost 90% and 70% of the fraction of probes for Er_2O_3 and Gd_2O_3, respectively, along the whole temperature range of measurement. The temperature dependence of the fitted hyperfine parameters for both interactions is displayed in Figure 3 for Er_2O_3 and Figure 4 for Gd_2O_3. These results show a near constancy of the fractions, asymmetry parameters
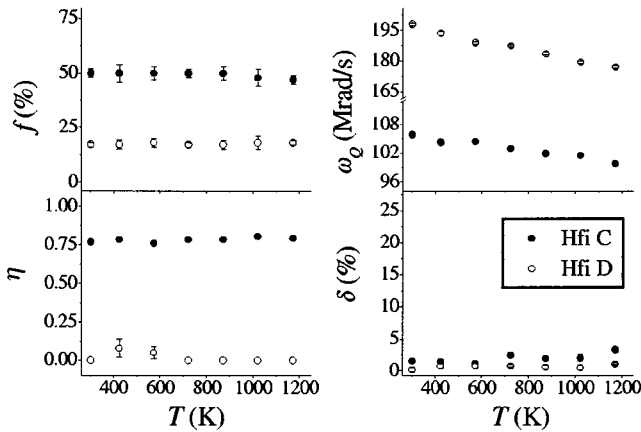
Fig. 4. Evolution of the hyperfine parameters of interactions Hfi C and Hfi D found in C-Gd_2O_3 as a function of the measuring temperature T.

and distributions, as well as a continuous diminution of the quadrupole frequencies.

For both sesquioxides additional hyperfine interactions were necessary to obtain the fits shown in Figures 1 and 2. In the case of Gd_2O_3, in addition to Hfi C and Hfi D, a third highly asymmetric hyperfine interaction labelled Hfi 3, characterized by $\omega_Q^3 = 126_1$ Mrad/s and $\eta^3 = 0.89_1$, gave account of 30% of the pattern. The fraction of Hfi 3 is rather constant along the whole temperature range, has a high distribution of 7% and already exists in the as-implanted stage. In the case of Er_2O_3 this third interaction amounts to only 3% at RT, around 10–14% in the rest of the temperature range and is characterized by $\omega_Q^3 = 108_2$ Mrad/s and $\eta^3 = 0.85_8$. A fourth interaction labelled Hfi 4 improved the fit results for this compound below 373 K, being characterized by $\omega_Q^4 = 117.2_9$ Mrad/s and $\eta^4 = 0.17_4$. This fraction gives account only for 6–9% of the pattern.

The XRD experiments performed in the Gd_2O_3 sample after the TDPAC measurements showed only the diffraction peaks of the cubic bixbyite phase. On the other hand, the XRD results corresponding to the Gd_2O_3 sample mixed with 10% of the high temperature B-phase clearly showed the diffraction peaks of the B-phase superimposed to those of the bixbyite cubic phase.

4 Discussion

4.1 Assignment of the hyperfine interactions

4.1.1 Main interactions

As has been shown, after the annealing of the samples the frequency distribution of both interactions is drastically diminished and the asymmetry parameter of Hfi D is reduced to zero (axial symmetry) as predicted by the coordination symmetry of cation site D. Moreover, the total fraction of both interactions accounts for more than 90% and 70% of the $R(t)$ pattern for Er_2O_3 and Gd_2O_3

respectively along the whole temperature range of measurement. After these major changes, Hfi C and Hfi D can be undoubtedly associated to the crystalline nonequivalent cationic sites called C and D in Section 2.2. In effect, these interactions have a very low frequency distribution pointing to a well-defined and stable configuration around the probe-atoms. The asymmetry parameters correspond to the expected symmetries and their values agree with the calculated ones (see Sect. 2.2). Furthermore, the frequency associated with the axially symmetric interaction is twice as large as the asymmetric one as found previously with the ^{181}Ta probe in Yb-, Y-, Dy-, Sm- and Lu-sesquioxides [7,12] and as predicted by PCM calculations. The continuous trend of Hfi C and Hfi D hyperfine parameters shown in Figures 3 and 4 as a function of the measuring temperature is a typical behaviour followed by probes in substitutional cation sites. Finally, the relative population of the two sites should be $f^C/f^D = 3$ if cationic sites were occupied according to their natural abundance in the structure. In the present experiments, $f^C/f^D = 3$ was found for Gd_2O_3. In the case of Er_2O_3, the experimental ratio f^C/f^D is smaller than this value. A departure of the tantalum (hafnium) relative occupancy of the crystallographic sites C and D is not surprising because similar behaviours have also been observed with the ^{181}Ta probe in previous studies of the bixbyite oxides and explained in terms of the relative ionic size of the probe and the cationic "space" of the host [18,23]. The present results for Er and Gd-sesquioxides are in good agreement with the occupancy trend previously observed.

4.1.2 Additional interactions

The Hfi 3 interaction found in Gd_2O_3 is very similar to one of the three interactions of ^{181}Ta in B-Gd_2O_3 (characterised by $\omega_Q^B = 120_3$ Mrad/s and $\eta^B = 0.85_4$ [24]). However this last interaction is not the more populated one found in Hf-implantation experiments in B-Gd_2O_3. If a small amount of the B-phase should be present in the bixbyite sample, the more populated of the three interactions (a fraction of 80% in B-Gd_2O_3) should be observed in our experiments. This fact is in agreement with the results of XRD experiments carried out in the sample used in the TDPAC experiments, which discard the existence of B-phase in the sample. On the other hand, we cannot discard the presence of embryos of the B-phase developing around the Hf impurities, perhaps with a higher coordination like in the B-phase. Another possibility, based on the hyperfine parameters of this interaction and its broad distribution, may be to correlate Hfi 3 with a distorted site C. This last interpretation is most probably the case of the third interaction in Er_2O_3 we already mentioned, taking into account their hyperfine parameters and the diminution of its fraction with temperature. The fourth interaction found in Er_2O_3 completely disappears above 473 K. Due to the involved temperatures and the hygroscopic tendency of rare-earth oxides, we thought that the presence of water might be at the origin of this interaction. However, differential thermal analysis (DTA)
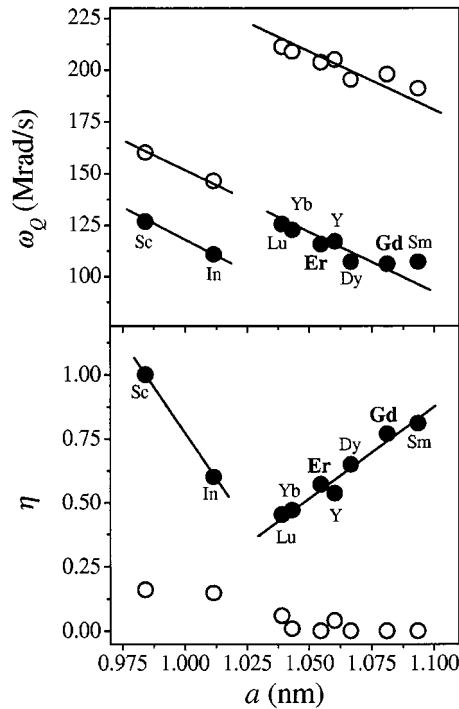
Fig. 5. Nuclear-quadrupole frequencies ω_Q and asymmetry parameters η for substitutional ^{181}Ta impurities at cation sites C (solid circles) and D (open circles) of the bixbyite structure as a function of the lattice parameter a.

experiments did not confirm this hypothesis. Finally, the high frequency responsible for the lost of amplitude at t = 0 in all the spectra could be correlated with the presence of probes located in grain boundaries or at the surface of the samples. Whatever the origin of these additional interactions, it should not affect the following discussion.

4.2 Substitutional sites C and D

We will center now the discussion in the two hyperfine interactions associated with the cationic sites C and D in the bixbyite structure of Er_2O_3 and Gd_2O_3, *i.e.*, Hfi C and Hfi D. First, we would like to compare the new results with the systematics found with ^{181}Ta in other bixbyite oxides [7,12,18,23]. As can be seen from Figure 5, the new data agree perfectly with the previous results, increasing the accuracy of the systematics. An important feature in this figure is the presence of a jump in the ω_Q values for both sites C and D (Fig. 5, top). This jump has been already discussed in reference [23]. In Figure 5 (bottom) we can now show that the local distortion in site D nearly preserve the axially symmetric environment of the probe.

The agreement of the new results with the ^{181}Ta systematics implies the confirmation of the already known trends when comparing ^{111}Cd and ^{181}Ta EFGs in bixbyites [7,23]. In effect, this very good agreement can be seen in the ratios between quadrupole interactions shown in Figures 6 and 7.
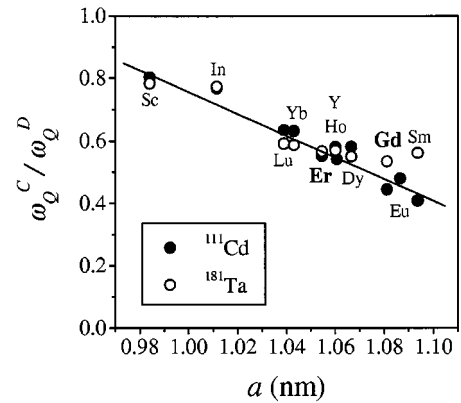

Fig. 6. Ratio of the nuclear-quadrupole frequency of site C to that of site D in bixbyites coming from TDPAC measurements using ^{111}Cd and ^{181}Ta as probes plotted as a function of the lattice parameter a. Experimental errors are smaller than the symbols. Solid line is a linear fit to the ^{111}Cd experimental data.
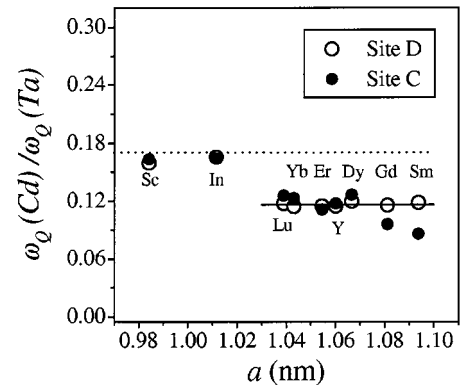

Fig. 7. ω_Q(Cd) / ω_Q(Ta) for sites C and D as a function of the lattice parameter a for the different bixbyite sesquioxides measured with the probes ^{111}Cd and ^{181}Ta. Experimental errors are smaller than the symbols. Dotted line: PCM prediction. The solid line is just to guide the eyes.

In order to compare the experimental trends with theoretical predictions in the frame of the PCM, we calculate the quadrupole frequency ω_Q^{PCM} for both nonequivalent cation sites using the crystallographic data of reference [21]. In Figure 8 we compare these results with the experimental ratio ω_Q^C/ω_Q^D for both probes shown in Figure 6. This comparison shows that the PCM alone is not adequate for describing the experimental ratios, especially at smaller lattice parameters. This is not surprising since the local EFG contribution (originated in the valence electrons of the probe atom) is not included in this kind of calculations.

On the other hand, the PCM predicts for the ratio ω_Q(Cd)$^{\text{Site }i}$/ω_Q(Ta)$^{\text{Site }i}$ a value of (dotted line in Fig. 7):

$$\frac{\omega_Q(\text{Cd})^{\text{Site }i}}{\omega_Q(\text{Ta})^{\text{Site }i}} = \frac{(1-\gamma_\infty)^{\text{Cd}}Q(\text{Cd})}{(1-\gamma_\infty)^{\text{Ta}}Q(\text{Ta})} = 0.1705, \quad (4)$$
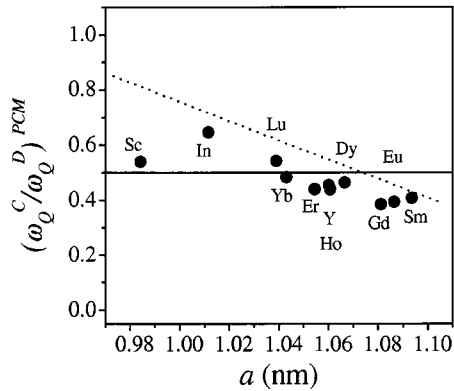
Fig. 8. Ratio of the nuclear-quadrupole frequency of site C to that of site D calculated with the point-charge model for the bixbyites presented in Figure 6 as a function of the lattice parameter a. Solid line: result for this relation in the idealised NN oxygen ions located at the corners of a perfect cube around sites C and D (see Sect. 2.2). Dotted line: linear fit to the ^{111}Cd experimental data plotted in Figure 6.

which is not in agreement with the experimental ratio shown in this figure (for a detailed discussion about In and Sc data see Ref. [23]).

The results obtained for the experimental ratios of Figures 6 and 7 can be explained as follows. The equality of the ratio ω_Q^C/ω_Q^D for Cd and Ta probes in each sesquioxide (see Fig. 6) shows that the dependence with the probe is cancelled. In addition, there is a remaining dependence of the EFG with the probe coordination geometry and the lattice parameter a (Fig. 6). On the other hand, the near constancy of $\omega_Q(\text{Cd})^C/\omega_Q(\text{Ta})^C$ and $\omega_Q(\text{Cd})^D/\omega_Q(\text{Ta})^D$ with a at each side of the jump (see Fig. 7) indicates that the dependence with the coordination geometry is also cancelled. The mismatch between the experiment and the PCM prediction shown in Figure 7 must be attributed to a remaining dependence with the electronic configuration of the probe. Hence, in order to explain both experimental ratios within the frame of the PCM and the Sternheimer antishielding approximation, the quadrupole frequency measured at a particular site with a certain probe ought to be written as:

$$\omega_Q^{\text{probe}\,i}(\text{Site}\,i) \propto$$
$$\mu^{\text{Site}\,i,\text{probe}\,i}(1 - \gamma_\infty)^{\text{probe}\,i}\,V_{ZZ}^{\text{lattice}}(\text{Site}\,i).\quad (5)$$

The factor μ is attributed to the local EFG produced by valence electrons of the probe atom and its nearest neighbours and must be factorised in two parts: one which depends on the geometry of the site and another that depends on the electronic configuration of the probe.

4.3 Temperature dependence of the EFG

The evolution of ω_Q and η with the measuring temperature T_m for ^{181}Ta probes located at both sites C and D were displayed in Figures 3 and 4. Within the errors, the temperature dependence of ω_Q^C, ω_Q^D and η^C is linear in T_m. In all cases, the slopes of the curves have an opposite sign

compared to those found in the ^{111}Cd TDPAC measurements [13]. In the case of η^D, no temperature dependence was observed.

In semiconductor and insulator systems, several temperature dependences have been observed, which have been explained in terms either of host properties or processes induced by the presence of the hyperfine probe [25, 26] that nearly always constitutes an impurity center in the host material. For this reason, we tried to estimate the influence of structural changes on the temperature dependence of the EFG in order to differentiate this contribution from electronic effects, as were found, for example, in C-Lu_2O_3 [27]. Isotropic lattice expansion always lead to a diminution in ω_Q. The magnitude of this variation can be evaluated through EFG calculations using the simple PCM. As far as we know, the only data on a temperature-dependent structural behaviour of C-Er_2O_3 and C-Gd_2O_3 are dilatometric expansion data [28]. An isotropic expansion of the lattice yields a calculated reduction in ω_Q for both sites C and D of about 2.4% and 2.5% in Er_2O_3 and Gd_2O_3, respectively, in the temperature range of 300–1073 K. The asymmetry parameter evidently does not change under the assumed isotropic expansion. These results are in poor agreement with the stronger decrease of the ω_Q values found in these experiments, *i.e.*, 8.8% (5.4%) and 8.9% (10.5%) for site C and D in Er_2O_3 (Gd_2O_3). We conclude that the isotropic expansion of the lattice cannot explain the temperature dependence of the EFG tensor at ^{181}Ta impurity located at both cationic sites of these oxides. Electronic aspects of the impurity-host entity, such as the impurity charge-state, should be considered in order to better described the EFG temperature dependence in these systems.

5 Conclusions

The characterisation of the nuclear-electric-quadrupole interaction of ^{181}Ta impurities at cation sites of the bixbyite structure of Er_2O_3 and Gd_2O_3 was achieved applying the TDPAC technique, subsequent to the implantation of ^{181}Hf ions into powder samples.

After the high-temperature annealing, both oxides show two very well-defined hyperfine interactions, which have been correlated to probes located at the two nonequivalent free-of-defects cation sites of the structure. The electric-field gradients at these sites agree perfectly with the systematics previously found in these compounds with the ^{181}Ta TDPAC probe. From the comparison of the present ^{181}Ta data with the already established ^{111}Cd systematics it has been shown that the EFG at ^{111}Cd and ^{181}Ta sites in bixbyites exhibit a strong dependence on the coordination geometry of the site and the electronic configuration of the probe. In addition, we present clear evidence that an ionic model alone, where the host is represented by point-charges and the impurity by the Sternheimer anti-shielding factor γ_∞, is not adequate for describing the obtained experimental results.

Concerning the temperature dependence of the hyperfine parameters that characterise the EFG's in the two

cationic sites of Er_2O_3 and Gd_2O_3, thermal lattice expansions are not enough to explain the observed decrease of ω_Q at both sites. As a consequence some additional effect (induced by the presence of the hyperfine probes) has to be considered in order to explain the experimental behaviour.

References

1. See, for example: S. Habenicht, D. Lupascu, M. Uhrmacher, L. Ziegeler, K.P. Lieb, and ISOLDE Collaboration, Z. Phys. B **101**, 196 (1996); M. Dietrich, D. Degering, J. Kortus, S. Unterricker, M. Deicher, A. Burchard, R. Magerle, and ISOLDE Collaboration, Hyperfine Interact. **120/121**, 359 (1999); A. Burchard, M. Deicher, V.N. Fedoseyev, D. Forkel-Wirth, R. Magerle, V.I. Mishin, D. Steiner, A. Stözler, R. Weissenborn, Th. Wichert, ISOLDE Collaboration, Hyperfine Interact. **120/121**, 389 (1999); M. Uhrmacher, K.P. Lieb, Z. Naturforch. **55 a**, 90 (2000).
2. D. Wiarda, M. Uhrmacher, A. Bartos, K.P. Lieb, J. Phys. Cond. Matt. **5**, 4111 (1992).
3. W. Bolse, A. Bartos, J. Kesten, M. Uhrmacher, K.P. Lieb, in *XXIII Zacopane School on Physics*, edited by K. Krolas, K. Tomala (Institute of Nuclear Physics, Cracow, 1988).
4. J. Kesten, W. Bolse, K.P. Lieb, M. Uhrmacher, Hyperfine Interact. **60**, 683 (1990).
5. M. Rentería, C.P. Massolo, A.G. Bibiloni, Mod. Phys. Lett. B **6**, 1819 (1992).
6. R. Weth, G. Fabricius, M. Weissmann, M. Rentería, C.P. Massolo, A.G. Bibiloni, Phys. Rev. B **49**, 14939 (1994).
7. M. Rentería, K. Freitag, L.A. Errico, Hyperfine Interact. **120/121**, 449 (1999).
8. M.S. Moreno, J. Desimoni, A.G. Bibiloni, M. Rentería, C.P. Massolo, K. Freitag, Phys. Rev. B **43**, 10086 (1991).
9. J.M. Adams, G. Catchen, Phys. Rev. B **50**, 1264 (1994).
10. J. Shitu, A.F. Pasquevich, J. Phys. Cond. Matt. **9**, 6313 (1997).
11. J. Luthin, K.P. Lieb, N. Neubauer, M. Uhrmacher, B. Lindgren, Phys. Rev. B **57**, 15272 (1998).
12. A.F. Pasquevich, A.G. Bibiloni, C.P. Massolo, M. Rentería, J.A. Vercesi, K. Freitag, Phys. Rev. B **49**, 14331 (1994).
13. EFG measurements with ^{111}Cd as probe in bixbyite-structure sesquioxides: In_2O_3: J. Desimoni, A.G. Bibiloni, L.A. Mendoza-Zélis, A.F. Pasquevich, F.H. Sánchez, A. López-García, Phys. Rev. B **28**, 5739 (1983); Y_2O_3: M. Uhrmacher, A. Bartos, K. Winzer, J. Less-Common Metals **150**, 185 (1989); Yb_2O_3, Dy_2O_3, and Sc_2O_3: A. Bartos, K.P. Lieb, A.F. Pasquevich, M. Uhrmacher, ISOLDE collaboration, Phys. Lett. A **157**, 513 (1991); Ho_2O_3, Gd_2O_3, and Sm_2O_3: J. Shitu, D. Wiarda, T. Wenzel, M. Uhrmacher, K.P. Lieb, S. Bedi, A. Bartos, Phys. Rev. B **46**, 7987 (1992); Eu_2O_3: A.F. Pasquevich, A.M. Rodríguez, H. Saitovich, P.R. de Jesus-Silva (unpublished); Er_2O_3: D. Lupascu, A. Bartos, K.P. Lieb, M. Uhrmacher, Z. Phys. B **93**, 441 (1994); Lu_2O_3: L.A. Errico, M. Rentería, A.G. Bibiloni, F.G. Requejo, Hyperfine Interact. **120/121**, 457 (1999).
14. H. Frauenfelder, R. Steffen, in α, β and γ-*Ray Spectroscopy*, Vol. 2, edited by K. Siegbahn (North-Holland, Amsterdam, 1968), p. 917.
15. A. Lerf, T. Butz, Hyperfine Interac. **36**, 275 (1987).
16. A.R. López-García, Magn. Res. Rev. **15**, 119 (1990).
17. L.A. Mendoza-Zélis, A.G. Bibiloni, M.C. Caracoche, A. López-García, J.A. Martínez, R.C. Mercader, A.F. Pasquevich, Hyperfine Interac. **3**, 315 (1977).
18. M. Rentería, F.G. Requejo, A.G. Bibiloni, A.F. Pasquevich, J. Shitu, K. Freitag, Phys. Rev. B **55**, 14200 (1997).
19. L. Eyring, *Handbook on the Physics and Chemistry of Rare Earth*, edited by K.A. Gschneider, L. Eyring (North-Holland, Amsterdam, 1979), p. 337.
20. B.M. Angelov, J. Phys. C **10**, L505 (1977); B.M. Angelov, J. Phys. C **15**, L239 (1982).
21. Crystal structure data used in PCM predictions. Two references are quoted if lattice parameters and atomic positions come from different articles (lattice parameter articles are quoted first). Er_2O_3: D. Lupascu, A. Bartos, K.P. Lieb, M. Uhrmacher, Z. Phys. B **93**, 441, (1994); Gd_2O_3: S. Stecura, W. Campbell, *Thermal Expansion and Phase Inversion of Rare Earth Oxides* (US Department of the Interior, Bureau of Mines Report of Investigations, 1961), p. 5847; A. Saiki, N. Ishizawa, N. Mizutani, M. Kato, Yogyo Kyokai Shi **93**, 649 (1985). Sc_2O_3: R.W.G. Wyckoff, *Crystal Structures*, Vol. 2, (Wiley Interscience, New York, 1964); R. Norrestam, Ark. Kemi, **29**, 343 (1968); In_2O_3: M. Marezio, Acta Cryst. **20**, 723 (1966); Y_2O_3, Dy_2O_3, and Ho_2O_3: E.N. Maslen, V.A. Streltsov, N. Ishizawa, Acta Cryst. B **52**, 414 (1996); Yb_2O_3: T. Schleid, G. Meyer, J. Less-Comm. Met. **149**, 73 (1989); Lu_2O_3, Eu_2O_3, and Sm_2O_3: S. Stecura, W. Campbell, *Thermal Expansion and Phase Inversion of Rare Earth Oxides* (US Department of the Interior, Bureau of Mines Report of Investigations, 1961) p. 5847; A. Saiki, N. Ishizawa, N. Mizutani, M. Kato, Yogyo Kyokai Shi **93**, 649 (1985).
22. F.D. Feiock, F.W. Johnson, Phys. Rev. B **39**, 187 (1969). In the case of Ta^{5+}, the value came from interpolation between the Hf^{4+} and W^{6+} values.
23. M. Rentería, A.G. Bibiloni, F.G. Requejo, A.F. Pasquevich, J. Shitu, L.A. Errico, K. Freitag, Mod. Phys. Lett. B **12**, 819 (1998).
24. M. Rentería, L.A. Errico, A.G. Bibiloni, K. Freitag (2000), unpublished.
25. D. Forkel, W. Engel, M. Iwatschenko-Borho, R. Keitel, W. Witthuhn, Hyperfine Interac. **15/16**, 821 (1983).
26. J. Shitu, A.F. Pasquevich, A.G. Bibiloni, M. Rentería, F.G. Requejo, Mod. Phys. Lett. B **12**, 281 (1998) and references therein.
27. L.A. Errico, M. Rentería, A.G. Bibiloni, F.G. Requejo, Hyperfine Interact. **120/121**, 457 (1999).
28. S. Stecura, W. Campbell, *Thermal Expansion and Phase Inversion of Rare Earth Oxides* (US Department of the Interior, Bureau of Mines Report of Investigations, 1961) p. 5847.